Fabrication of Photonic Crystal Structures on GaAs by Single Pulse Laser Interference Lithography

Zhiheng Lin, Yaoxun Wan[1], Yun-Ran Wan[1], Im Sik Han, and Mark Hopkinson[*]

Department of Electronic and Electrical Engineering, University of Sheffield. North Campus, Broad Lane. Sheffield. S3 7HQ. United Kingdom
[*]Corresponding author's e-mail: m.hopkinson@sheffield.ac.uk

Photonic crystal (PhC) structures generated through periodic surface nanostructuring are pivotal for controlling light-matter interactions. These structures are essential for reducing high surface reflectivity in semiconductor optical devices, enhancing light absorption in photovoltaic cells, and improving light extraction in LEDs. Although various methods for PhC fabrication are well-documented, the use of single-pulse laser interference lithography (LIL) with commercial photoresists remains unexplored. Single nanosecond pulses for photoresist exposure offer significant advantages, including high throughput for large-scale patterning and reduced dependence on stable optical platforms. In this study, we used single-pulse LIL to fabricate antireflective PhC structures on GaAs substrates using a commercial photoresist. This process involved exposing the photoresist to single 7 nanosecond pulses at a wavelength of 355 nm, with relatively low energy levels. High-quality nanohole arrays were subsequently created via inductively coupled plasma (ICP) etching. Reflectivity analysis revealed that these structures reduced the average reflectance of GaAs to below 5% across the visible wavelength range of 450-700 nm. This work is crucial for optimizing current photonic technologies and advancing future devices with enhanced light management capabilities.
DOI: 10.2961/jlmn.2024.02.2007
Keywords: photonic crystal, laser interference lithography, antireflection, semiconductors, optical devices.

1. Introduction

Surface nanostructuring has emerged as a pivotal technique for enhancing the absorption and extraction of light in semiconductor optical devices such as solar cells, light-emitting diodes (LEDs), and laser diodes (LDs) [1-4]. A significant challenge in these devices is the high surface reflectivity, which leads to reduced photoelectric conversion efficiency and, consequently, wasted energy. For instance, a commonly used semiconductor material GaAs, exhibits reflectivity exceeding 39% in the visible spectrum. This high reflectivity limits the power conversion efficiency of GaAs solar cells to around 17.57% and constrains the external radiation efficiency of GaAs LEDs to merely 3% [5,6].

Given this context, reducing surface reflectivity in semiconductor optical devices has garnered substantial research interest. Two primary methods are employed to alter surface reflectivity: bottom-up approaches, such as antireflective coatings (ARCs) [7-9], and top-down approaches, including surface nanostructuring [10-12]. ARCs are instrumental in enhancing visible spectrum transmittance and mitigating surface reflection losses and angular reflectivity dependence, which are critical for improving the light extraction efficiency in LEDs and the contrast and brightness in display technologies. However, achieving wideband antireflectance with ARCs necessitates meticulous material selection with specific refractive indices and precise calibration of layer thicknesses, thus complicating the fabrication process and increasing time consumption during both development and manufacturing phases [13-16].

Alternatively, surface nanostructuring provides a gradual refractive index transition between air and the semiconductor material, minimizing Fresnel reflections and increasing light entry into the semiconductor. Nanostructures like 'Moth Eye' configurations can significantly reduce spectral reflectance across a broad range, from the visible spectrum (approximately 400 nm) to the mid-infrared region (up to 11 μm), achieving average reflectance below 2% [17,18]. Moreover, Photonic crystals (PhC), with their periodic nanostructures, further extend the capabilities of light manipulation beyond antireflection, facilitating innovative technological applications in LEDs, solar cells, telecommunications, sensors, and other optical devices [19-22].

Several methods have been developed for the synthesis of PhC structures, including electron beam lithography (EBL) [23,24] and nanoimprint lithography (NIL) [25,26]. Although effective, these techniques often have high costs. In contrast, laser interference lithography (LIL) is praised for its simplicity, cost-efficiency, and temporal efficiency, enabling rapid fabrication and large-area patterning suitable for industrial-scale production. Previous studies have employed some LIL methods such as direct LIL to fabricate PhC structures and using two-beam LIL for multiple exposures to achieve the desired PhC configurations. However, the application of three-beam single-pulse LIL for the fabrication of PhC nanostructures is scarcely documented in the literature [27-29].

In this study, we employ single-pulse three-beam LIL to fabricate PhC structures on GaAs substrates, followed by inductively coupled plasma (ICP) etching to create nanoholes

of varying depths. By adjusting the LIL settings, we produced three sets of PhC structures with different sizes, demonstrating the technique's flexibility. Our findings indicate that these surface PhC nanoholes significantly enhance light extraction and trapping capabilities within their corresponding wavelength ranges by simulating the photonic band gap (PBG). Furthermore, surface reflectivity measurements reveal a substantial decrease in average reflectance, with values dropping below 5% across the visible wavelength range of 400-700 nm. This investigation aims to understand how integrating PhC affects reflectivity, revealing the mechanisms behind the enhanced optical performance these nanostructures provide. Such insights are essential for optimizing current photonic technologies and advancing future devices with superior light management capabilities.

2. Experimental details

2.1 Laser interference lithography system

In this study, the LIL system is central to the experimental setup. It employs a flash-lamp pumped Nd:YAG laser (Innolas Spitlight) with the following parameters: wavelength of 355 nm, frequency of 5 Hz, pulse duration of 7 ns, and beam diameter of 6 mm. The initial laser beam has a top hat profile with an m^2 value of about 1.2, but some propagation to gaussian occurs along the ≤ 1m optical path.

This laser generates interference patterns by splitting the beam into three equal parts using beam splitters. The use of three beam LIL can avoid Moiré pattern effects typical of four-beam or more than four-beam setups [30]. The three beams are then recombined on the sample surface, where they interfere constructively and destructively, creating a periodic pattern of light and dark regions due to the variations in the intensity of the electric field, thus exposing the photoresist to create the desired pattern. The final PhC structure is defined by this pattern, governed by Equation 1. In Equation 1, I represents the intensity of the interference pattern, m is the number of beams, A_m denotes the amplitude, $\overrightarrow{P_m}$ is the unit polarization vector, $\overrightarrow{k_m}$ is the wave vector indicating the propagation direction, $\vec{r}$ is the position vector, and δ_m is the initial phase.

$$I = \left|\sum_{i=1}^{n} A_m \overrightarrow{P_m} exp\left[i\left(\overrightarrow{k_m} * \vec{r} + \delta_m\right)\right]\right|^2 \quad (1)$$

Equation 2 relates the pitch (P) of the interference pattern to the angle of incidence (θ) of the laser beams. λ is the wavelength of the laser.

$$P = \frac{\lambda}{\sqrt{2}\sin\theta} \quad (2)$$

2.2 Fabrication process of the PhC structure

The experimental process is shown in Figure 1. GaAs substrates (Fig 1a) underwent a three-step cleaning protocol before applying a 180 nm-thick film of mr-P 1200LIL photoresist (Micro resist technology GmbH) through spin-coating as shown in Fig 1b. This photoresist, specifically designed for laser lithography applications, offers high contrast for thin film applications. Previous attempts with standard lithography photoresists at greater thicknesses were unsuccessful due to incomplete exposure depth and residuals that could not be fully removed through etching. Although deeper exposure can be achieved with higher laser pulse power, this increases the risk of laser-induced damage to the photoresist. The thin, high-contrast mr-P 1200LIL photoresist is thus suitable for complete etching with lower energy single-pulse LIL. This photoresist was exposed to single pulse three-beam LIL to define the desired pattern. After that, pattern transfer on GaAs samples was achieved through ICP etching at a rate of 200 nm per minute (see Fig 1c). By controlling the etching duration, we successfully fabricated PhC structures with various etch depths. The final step is to wash out the photoresist using a three-step cleaning protocol after which we obtain GaAs samples with PhC structure as shown in Fig 1d.

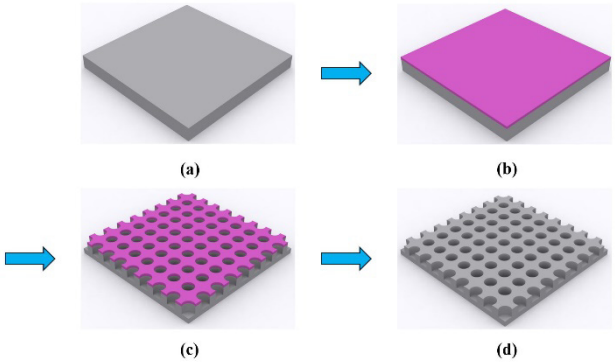

Fig. 1 The fabrication process of the PhC structures.

3. Results and discussion

3.1 The SEM results analysis

The Scanning electron microscope (SEM) analysis reveals the characteristics of the fabricated PhC structures under varying conditions. When the angle of incidence for the three beams is set to 30° (θ= 30º) and the azimuth angles are 0°, 90°, and 180°, the resulting PhC structure is shown in Figures 2a and 2b. The pitch between the nanoholes measures approximately 500 nm, consistent with the predictions of Equation 2. The diameter of each nanohole is influenced by the laser energy used during the lithographic process. Figure 2a, produced with a laser energy of 9 mJ. Inadequate laser intensity can result in incomplete exposure of the photoresist, leaving residual material that impedes effective etching. Conversely, excessive laser intensity can cause adjacent nanoholes to merge, disrupting the PhC structure. As shown in Figure 2b, with a laser energy of 12 mJ, the gap between nanoholes becomes more narrow.

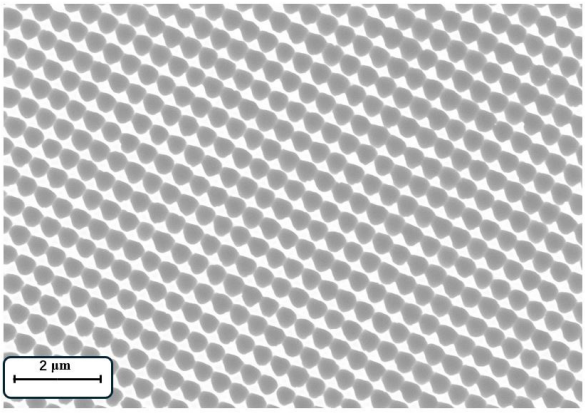

(a)

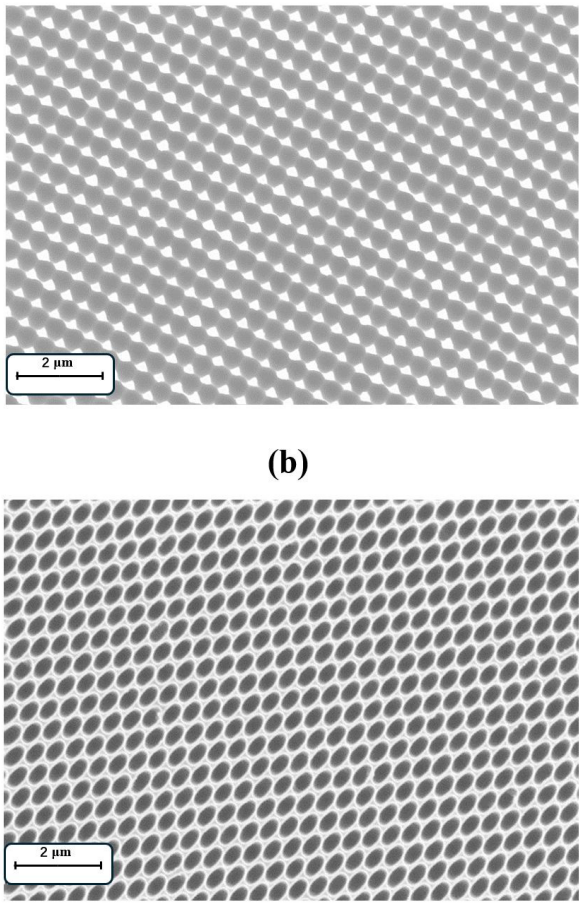

Fig. 2 The SEM images of PhC structures with **a)** 417 nm diameter and 500 nm pitch, **b)** 440 nm diameter and 500 nm pitch, **c)** 315 nm major axis, 305 nm minor axis and365 nm pitch.

For light-emitting devices, it is crucial that the PBG windows of the PhC structure correspond to the emission wavelength. Achieving this requires a smaller pitch. By adjusting the angle of incidence of the three beams to 43° (θ= 43º) while keeping the azimuth angles unchanged, we obtained the SEM result shown in Figure 2c, with a pitch of approximately 365 nm. Manipulating the radius of the holes (r) relative to the pitch (P), along with considering the refractive index contrast between the holes and the surrounding membrane, allows for control over the PBG characteristics. Specifically, a smaller r/P ratio results in a narrower PBG, which increases linearly with this ratio. Increasing the air content in the structure by enlarging the radius raises the central bandgap frequency. However, a larger radius increases loss rates due to reduced guiding material and fabrication complexity. Therefore, a laser energy of 9 mJ was chosen to achieve a balance, resulting in more satisfactory PhC structures with elliptical nanoholes, where the major axis is approximately 315 nm and the minor axis is approximately 305 nm.

Figure 3 presents the simulation outcomes of the PBG using the FDTD method. This simulation aligns with the SEM data regarding the size and pitch of the nanoholes. The dispersion diagram indicates PBGs in two spectral regions: between normalized frequencies of 0.28 to 0.31 and from 0.38 to 0.44. These results suggest that the 2D PhC structure operates efficiently as an out-coupler for transverse electric (TE) guided modes within its active range from 830 nm to 960 nm and 1177 nm to 1303 nm. The significance of these wavelength ranges is underscored by their correspondence with the emission wavelengths of various GaAs based semiconductor devices. Specifically, the range from 830 nm to 960 nm aligns with the emission wavelengths typical of GaAs/InGaAs-based LEDs and LDs. Additionally, the longer wavelength range from 1177 nm to 1303 nm corresponds to the O-band, which is recognized for its reduced dispersion and attenuation in optical fibers.

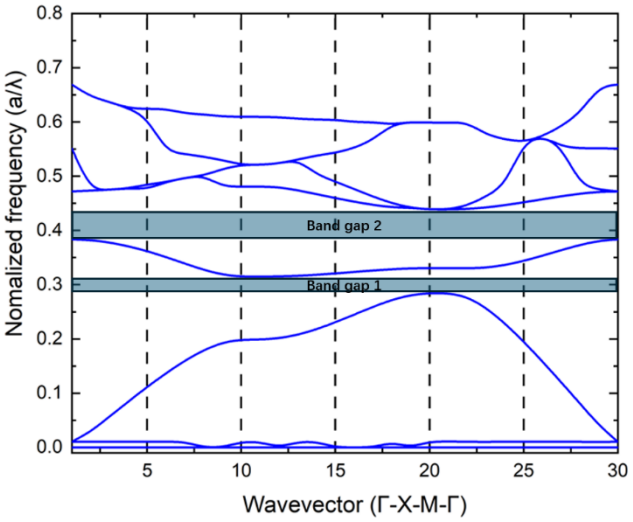

Fig. 3 The PBG for the 2D PhC obtained from FDTD.

3.2 Reflectance results analysis

The reflectance of all fabricated PhC structures at varying depths was characterized using a silicon CMOS array detector spectrometer (ASEQ Instruments) integrated into an optical microscope with visible illumination ranging from 450 nm to 700 nm. This setup, previously reported [31], enables the measurement of reflectance for each pattern at different depths. Precise positioning of the sample is ensured by a panning stage, allowing for accurate measurements through the microscope. Illumination was focused on the pattern area using the microscope's aperture control. For this study, a 50X microscope objective with a numerical aperture (NA) of 0.56 and a 33.3° half-cone angle was employed, using an NA of up to 1 or a 100X microscope objective.

We compared the reflectivity properties of GaAs substrates with and without embedded PhC structures at various depths, fabricated using ICP etching. Samples of different etch depth do not show significant variation of the PhC diameter as a consequence of the high directionality of the ICP etch.

The reflectance spectra of these samples are illustrated in Figure 4. Data in Figure 4a corresponds to a PhC structure with a pitch of 500 nm and a diameter of 417 nm, Figure 4b shows data for a pitch of 500 nm and a diameter of 440 nm, and Figure 4c presents data for a pitch of 365 nm and a diameter of approximately 310 nm. The bare GaAs substrate exhibited a high average reflectance, up to 39%, within the wavelength range of 450 nm to 700 nm. This high reflectance is due to the refractive index contrast between air and GaAs, which has a refractive index of approximately 3.8.

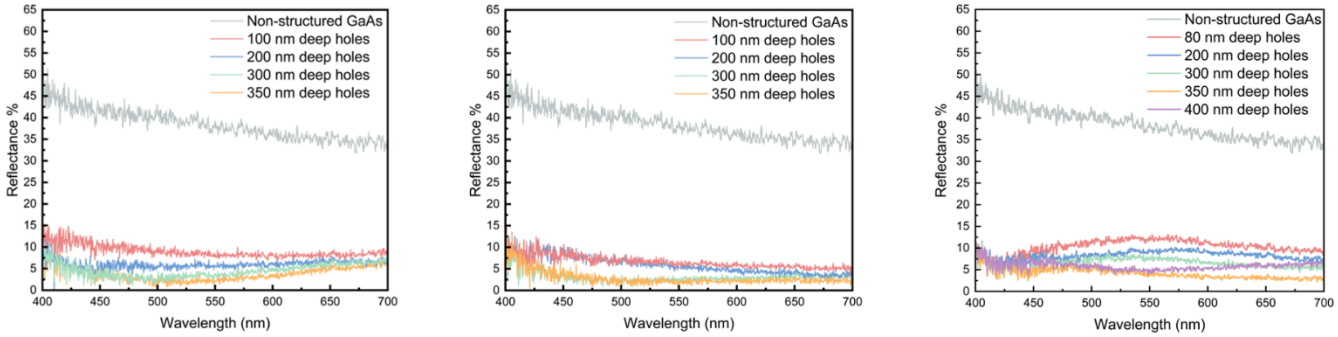

Fig. 4 Comparative analysis of reflectance between bare GaAs substrates and GaAs substrates embedded with PhC structures **a)** 417 nm diameter and 500 nm pitch, ranging in depths from 100 nm to 350 nm; **b)** 440 nm diameter and 500 nm pitch, ranging in depths from 100 nm to 350 nm; **c)** 315 nm major axis, 305 nm minor axis and365 nm pitch, ranging in depths from 80 nm to 400 nm.

A key observation was the impact of PhC structure depth on reflectivity. Reflectance data in Figure 4 indicates a trend in which increasing the depth of nanoholes correlates with reduced reflectivity. When nanohole depth reached 350 nm, the average reflectance decreased to below 5% across the spectral range of 400 nm to 700 nm, representing a sevenfold reduction compared to bare GaAs. This reduction is attributed to enhanced light trapping as incident light traverses a longer path within the material, increasing the probability of absorption. Additionally, deeper PhC structures optimize Bragg scattering, causing diffraction that leads to constructive or destructive interference, effectively reducing surface reflectance. These diffraction effects can also redirect light away from the surface, further lowering reflectivity.

However, there are limits to this trend. As shown in Figures 4a and 4b, reflectivity stabilizes once the depth reaches 300 nm. In Figure 4c, at depths of 400 nm, reflectivity exhibited a slight increase rather than a continuous decline. This suggests that excessive depth may negatively impact light trapping or introduce unwanted diffraction effects, altering reflectivity in undesired ways.

4. Conclusion

In this study, we successfully designed and fabricated various PhC structures on GaAs substrates using the single pulse LIL technique. The surface morphology of the fabricated PhC structures was confirmed through SEM analyses, aligning with our design expectations. FDTD simulations were performed to characterize the PBG properties of these structures, revealing their potential for integration into GaAs-based optoelectronic devices. This integration is anticipated to enhance device performance by providing gain within specific wavelength ranges. Our experimental measurements indicated that the average reflectance of GaAs substrates with PhC structures was significantly reduced to below 5% across a broad wavelength spectrum of 450 nm to 700 nm. These findings suggest that the PhC structures developed in this research can significantly improve light extraction efficiency in light-emitting devices and enhance light trapping efficacy in photovoltaic applications. The adaptability of single pulse LIL to various semiconductor materials highlights its potential for creating highly efficient optoelectronic devices optimized for broadband applications. This cost-effective and high-throughput technology holds significant promise for advancing the field of photonics and optoelectronics, contributing to technological progress in these areas.

Acknowledgments and Appendixes

The authors gratefully acknowledge financial support from EPSRC (Grant: EP/X016838/1) and the Grantham Foundation Opportunities Fund.

References

[1] S.M. Ko, J. Hur, C. Lee, Isnaeni, S.H. Gong, M.K. Kim, and Y.H: Cho, Sci. Rep., 10, (2020) 358.
[2] D. Allemeier, B. Isenhart, E. Dahal, Y. Tsuda, T. Yoshida, and M.S. White: Nature Commun., 12, (2021) 6111.
[3] K. Emoto, T. Koizumi, M. Hirose, M. Jutori, T. Inoue, K. Ishizaki, M. De Zoysa, H. Togawa, and S. Noda: Commun. Mater., 3, (2022) 72.
[4] S. Almenabawy, Y. Zhang, A. Flood, R. Prinja, and N.P. Kherani: ACS Appl. Energy Mater., 5, (2022) 13808.
[5] D. Parajuli, G.S. Gaudel, D. Kc, and K.B. Khattri: AIP Adv., 13, (2023) 085002.
[6] T.C. Lin, Y.T. Chen, Y.F. Yin, Z.X. You, H.Y. Kao, C.Y. Huang, Y.H. Lin, C.T. Tsai, G.R. Lin, and J.J. Huang: IEEE Trans. Electron Devices, 65, (2018) 4375.
[7] W. Zhang, K. Hu, J. Tu, A. Aierken, D. Xu, G. Song, X. Sun, L. Li, K. Chen, D. Zhang, and Y. Zhuang: Solar Energy, 217, (2021) 271.
[8] G.J. Hou, I. García, and I. Rey-Stolle: Solar Energy, 217, (2021) 62.
[9] M.A. Zahid, M.Q. Khokhar, Z. Cui, and H. Park: Results Phys., 28, (2021) 104640.
[10] S. Ji, K. Song, T.B. Nguyen, N. Kim, and H. Lim: ACS Appl. Mater .Interfaces, 5, (2013) 10731 .
[11] F. Galeotti, F. Trespidi, G. Timò, and M. Pasini: ACS Appl. Mater. Interfaces, 6, (2014) 5827.
[12] Y.-J. Hung, S.-L. Lee, and L.A. Coldren: Optics Express, 18 (2010) 6841.
[13] M.A. Zahid, M.Q. Khokhar, S. Park, S.Q. Hussain, and Y. Kim: Vacuum, 200, (2022) 110967.
[14] M.A. Zahid, M.Q. Khokhar, and Y. Kim: Crystal Research and Technology, 57, (2022) 2100233.
[15] Y.S. Lee, L.Y. Chuang, C.J. Tang, Z.Z. Yan, and B.S. Le: Crystals (Basel), 13, (2023) 80.
[16] N. Sahouane and A. Zerga: Energy Procedia, 44 (2014), 118.

[17] L. Dong, Z. Zhang, R. Ding, L. Wang, M. Liu, Z. Weng, and Z. Wang: Surf. Coat. Technol., 372, (2019) 327.
[18] L. Dong, Z. Zhang, L. Wang, Z. Weng, M. Ouyang, Y. Fu, J. Wang, and D. Li: Appl. Opt., 58, (2019) 6706.
[19] T. Sridarshini and S. Indira Gandhi: Laser Phys., 30, (2020) 116206.
[20] L. Suslik, D. Pudis, M. Goraus, R. Nolte, J. Kovac, J. Durisova, P. Gaso, P. Hronec, P. Schaaf: Appl. Surf. Sci., 395, (2017) 220.
[21] M.A. Husanu, C.P. Ganea, I. Anghel, C. Florica, O. Rasoga, and D.G. Popescu: Appl. Surf. Sci., 355, (2015) 1186.
[22] H. Kaviani and J. Barvestani: Appl. Surf. Sci., 599, (2022) 153743.
[23] S.P. Yu, D.C. Cole, H. Jung, G.T. Moille, and K. Srinivasan: Nature Photonics, 15, (2021) 461.
[24] J. Li, J. Yan, L. Jiang, J. Yu, and H. Guo: Light Sci. Appl., 12, (2023).
[25] K.J. Byeon, S.Y. Hwang, and H. Lee: Appl. Phys. Lett. 91, (2007) 091106.
[26] H. Zhao, X. Cao, Q. Dong, C. Song, and L. Wang: Nanoscale Adv., 5, (2023) 1291.
[27] D. Pudis, L. Suslik, J. Skriniarova, J. Kovac, J. Kovec, I. Kubicova, I. Martincek, S. Hascik, and P. Schaaf: Appl. Surf. Sci., (2013), 161
[28] X. Tang, L. Wang, M. Zhao, W. Huo, L. Han, Z. Deng, Y. Jiang, W. Wang, and H. Chen: Optics Communications., 481, (2021) 126539.
[29] P. Zuo, B. Zhao, S. Yan, G. Yue, H. Yang, Y. Li, H. Wu, Y. Jiang, H. Jia, J. Zhou, and H. Chen: Optical and Quantum Electron., 48(5), (2016) 288.
[30] Y.R. Wang, I.S. Han, C.Y. Jin, and M. Hopkinson: ACS Appl. Nano. Mater., 3, (2020) 4739.
[31] S. Behera, P.W. Fry, H. Francis, C.Y. Jin, and M. Hopkinson: Sci. Rep., 10, (2020) 6269.

(Received: June 8, 2024, Accepted: September 15, 2024)